

The Effect of Hydrogel Injection on Cardiac Function and Myocardial Mechanics in a Computational Post Infarction Model

Jeroen Korttsmit (1), Neil H. Davies (1), Renee Miller (1),
Jesse R. Macadangdang (1,2), Peter Zilla (1) and Thomas Franz (1,3,4)

1. *Cardiovascular Research Unit, Chris Barnard Division of Cardiothoracic Surgery, University of Cape Town, South Africa*
2. *Department of Biomedical Engineering, University of Virginia, USA*
3. *Centre for Research in Computational and Applied Mechanics, University of Cape Town, South Africa*
4. *Centre for High Performance Computing, South Africa*

Corresponding authors:

Jeroen Korttsmit, PhD
Cardiovascular Research Unit
Chris Barnard Building, Room 2.15
Faculty of Health Sciences
University of Cape Town
Anzio Road
Observatory 7925
Cape Town
South Africa
Tel: +27 21 406 6418
Fax: +27 21 448 5935
Email: jeroen.korttsmit@uct.ac.za

Thomas Franz, PhD
Cardiovascular Research Unit
Chris Barnard Building, Room 3.09
Faculty of Health Sciences
University of Cape Town
Anzio Road
Observatory 7925
Cape Town
South Africa
Tel: +27 21 406 6418
Fax: +27 86 684 7288
Email: thomas.franz@uct.ac.za

In press as:

Korttsmit J, Davies NH, Miller R, Macadangdang JR, Zilla P, Franz T. The effect of hydrogel injection on cardiac function and myocardial mechanics in a computational post-infarction model. *Comput Methods Biomech Biomed Eng*, 2012.

Abstract

An emerging therapy to limit adverse heart remodelling following myocardial infarction is the injection of polymers into the infarcted left ventricle (LV). In the few numerical studies performed in this field, the definition and distribution of the hydrogel in the infarcted myocardium was simplified. In this computational study, a more realistic biomaterial distribution was simulated after which the effect on cardiac function and mechanics was studied. A validated FE heart model was employed in which an antero-apical (AA) infarct was defined. Four infarct models were created representing different temporal phases in the progression of a myocardial infarction. Hydrogel layers were simulated in the infarcted myocardium in each model. Biomechanical and functional improvement of the LV was found after hydrogel inclusion in the ischemic models representing the early phases of myocardial infarction. In contrast, only functional but no mechanical restitution was shown in the scar model due to hydrogel presence.

Keywords: myocardial infarction; injection therapy; hydrogel; FE model.

1. Introduction

Cardiovascular diseases are the world's largest killers, claiming 17.1 million lives a year. By 2030, it is expected that almost 23.6 million people will die from cardiovascular diseases, mainly from heart disease and stroke (Cardiovascular diseases (CVDs) - Key Facts 2011). A dramatic increase in cardiovascular disease incidences is expected in Africa, in conjunction with improvement of economic wealth and social environment and the emergence of obesity, diabetes and uncontrolled hypertension (Steyn et al. 2005).

Of all cardiovascular pathologies, myocardial infarction has been presented as the most common cause of heart failure (Heart disease 2008). Myocardial infarction (MI) is the death of myocardium caused by the occlusion of the coronary artery which supplies oxygen and nutrients to the infarcted region. Immediately after occlusion, the infarcted myocardium converts from an active, contractile tissue to a passive non-contractile material. This results in an increase in loading of the heart that induces a unique pattern of remodelling of the infarcted and non-infarcted myocardium. A cascade of biochemical intracellular signalling processes is triggered that initiates and, subsequently, regulates reparative changes which include dilatation, hypertrophy and the formation of a discrete collagen scar (Sutton and Sharpe 2000; Holmes et al. 2005). Ventricular remodelling may continue for weeks or months but since these intrinsic mechanisms of repair often fail to fully restore the heart function, they may lead to a downward spiral into end-stage heart failure. Ventricular dilation is strongly related to poor outcomes following myocardial infarction (Tischler et al. 1993; White et al. 1987) and is propagated by a positive feedback loop with LV wall stress (Pfeffer and Pfeffer 1987; Pfeffer and Braunwald 1990).

Many therapies try to limit the adverse remodelling of the heart by using mechanical approaches to attenuate cardiac dilation, restore geometry and decrease heart wall stress. These treatments can be divided into highly invasive surgical procedures which have shown some clinical efficacy even in chronic heart failure patients (Guccione et al. 2003; Klodell Jr et al. 2008), and into the use of injectable biomaterials whose application and research have grown over the past decade (Nelson et al. 2011; Kawamoto et al. 2003). Intra-myocardial biomaterial injection therapy has been inferred to have acute functional benefits on cardiac

function and myocardial wall stress (Nelson et al. 2011). Nevertheless, to elucidate the specific mechanisms behind these functional improvements and to increase the potential of this therapy, more research is needed. The optimization of biomaterial properties, such as mechanical properties and biodegradability, and the number of injections, volume, location and the timing of delivery after infarction seem to be most in need of investigation.

The finite element (FE) method is well suited to address these issues. It has been shown to be the perfect tool to capture many aspects of LV mechanics with a representative 3-dimensional geometry and the definition of both contractile and passive material properties. Previous FE studies have validated computational predictions by indicating good agreement with myocardial strains measured with implanted markers or tagged magnetic resonance imaging (MRI) (Bovendeerd et al. 1996; Guccione et al. 1991; Omens et al. 1993). However, only a few computational studies have been performed in which the short-term mechanical effects of post-infarct biomaterial injection into the myocardium were investigated.

Wall et al. (2006) investigated single and multiple border zone injections and single injection into the infarct zone with a range of injection volumes and various mechanical properties of the injected material. A validated FE model of an ovine LV with an antero-apical (AA) infarct was used which was previously proposed by Walker et al. (2005). Material injection was represented by local adjustment of the FE mesh. Biomaterial properties were not defined independently but by applying a volume-mixing rule to alter the overall mechanical properties and contractility of the myocardium due to biomaterial incorporation. Results showed that material injection in the infarct border zone reduced end-systolic LV fibre stresses. This attenuating effect on wall stress increased with the fractional volume added and the stiffness of the injected material. Furthermore, material injection resulted in a slight increase in ejection fraction (EF), but another indicator of cardiac function, stroke volume divided by LV end diastolic pressure, was unchanged. Wenk et al. (2009) developed a finite element (FE) based method to optimize the injection pattern of spherical polymeric inclusions according to a specific objective function. Both myofibre stress and stroke volume were incorporated into the objective function with different weights. Material properties were defined by a pseudo-elastic strain energy function and a time-varying elastance model of active contraction (Guccione et al. 1991, 1995). Infarcted tissue was not defined in the model with the diseased state of the heart being represented only by its dilated geometry. Results indicated that as the number of inclusions increased, the mean myofibre stress in the LV decreased both at end-diastole and end-systole. However, the incorporation of both stress and stroke volume together in the objective function led to a result that deviated from the maximum number of inclusions. The main limitation of both FE studies is that the biomaterials injected into the myocardium were modelled in a simplified fashion that was not based on experimental work and did not provide a micro-structural representation of the distribution of the material in the myocardium.

Hence, the objective of this study is to model a more realistic distribution of the incorporated hydrogel in the infarcted LV heart wall, and to investigate the effect of the included hydrogel on cardiac functionality and myofibre mechanics. To reach this goal, a previously developed canine FE model was used in which large LV antero-apical (AA) infarcts were simulated. Different infarct models were created by changing the mechanical properties of the infarcted tissue according to the development of a myocardial infarction in time (Holmes et al. 2005). In this way, four models were developed representing three ischemic infarct stages and one scarred infarct. Biomaterial dispersion in the infarcted wall was simulated as multiple thin layers to approximate the layered distribution of the injected biomaterial observed in previous experimental studies (Dobner et al. 2009; Ifkovits et al. 2010). Cardiac functional parameters, myofibre stresses and strains were calculated and evaluated for each infarct model with and without incorporation of the hydrogel layers.

2. Materials & Methods

To study the effect of hydrogel inclusion in the infarcted LV wall, the software package Continuity®6.3b (University of California in San Diego, CA, USA) was used in which a 3D finite element (FE) ventricular model is coupled to a lumped parameter systems model of the circulation (Kerckhoffs et al. 2007). A pre-existing canine heart model was employed that featured a left and right ventricular geometry including the 3D myofibre angle distribution (Nielsen et al. 1991). The FE mesh was created from the unloaded, resting heart and cavity volumes were equal to 26.1 and 22.3 ml for the left and right ventricle, respectively. The initial mesh consisted of 48 tricubic Hermite elements in a 4x3x4 grid (circumferential x longitudinal x transmural). For the purpose of the current study, the initial mesh described above was refined in the transmural direction to increase the number of element layers between the left ventricle endocardium and the epicardium.

2.1 Constitutive models

Passive myocardium (during diastolic filling) was modelled using a nearly incompressible, transversely isotropic strain energy function W :

$$W = \frac{1}{2} C(e^Q - 1) + C_{\text{compr}}(I_3 \ln I_3 - I_3 + 1) \quad (1)$$

in which

$$Q = b_{ff} E_{ff}^2 + b_{cc}(E_{cc}^2 + E_{ss}^2 + E_{cs}^2 + E_{sc}^2) + b_{fc}(E_{fs}^2 + E_{sf}^2 + E_{fc}^2 + E_{cf}^2) \quad (2)$$

where E_{ff} is the fibre strain, E_{cc} is cross-fibre in-plane strain, E_{ss} is the radial strain transverse to the fibre, E_{cs} is the shear strain in the transverse plane, and E_{fc} and E_{fs} are shear strain in fibre – cross-fibre and fibre – radial coordinate planes, respectively. The diastolic myocardial material parameters; stress-scaling coefficient $C = 0.88$ kPa, $b_{ff} = 18.5$, $b_{cc} = 3.58$ and $b_{fc} = 1.63$ were determined previously for healthy canine myocardium (Guccione et al. 1991). The last term of the strain energy function W , Equation (1) represents the penalty function to model the passive myocardium as nearly incompressible. C_{compr} is the bulk modulus of the tissue and was set to 100 kPa, while I_3 represents the volume ratio (determinant) of the stretch tensor \mathbf{U} (Usyk et al. 2000).

Active myocardium (during systolic contraction) was modelled as the sum of the passive stress derived from the strain energy function, Equation (1), and an active fibre directional component (T_0). The latter is a function of time (t), peak intracellular calcium concentration (Ca_0), sarcomere length at which no active tension develops (l_0), stress-free sarcomere length (l_R), and maximum isometric tension achieved at the longest sarcomere length (T_{max}). The material constants for active contraction were set to the following values as previously described; $Ca_0 = 4.35$ $\mu\text{mol/l}$, $l_0 = 1.58$ μm , $l_R = 1.85$ μm , and $T_{\text{max}} = 135.7$ kPa (Guccione et al. 1993).

2.2 Infarct models & hydrogel inclusion

To study the effect of myocardial infarction and hydrogel injection on cardiac performance and biomechanics, a reference model of the healthy heart and models of a heart with antero-apical (AA) myocardial infarct (Figure 1) with different constitutive properties of the infarct region were generated. The infarct models were classified according to the chronological

development of a healing myocardial infarct after occlusion of the left anterior descending (LAD) artery supplying the AA region of the heart. AA ischemic infarct model 1 (II_1) represents the time period immediately after occlusion of the coronary artery. In this phase of the healing process, the mechanics of the infarcted region are dominated by the conversion of the myocardium from active, force-generating material to a passive non-contractile tissue (Holmes et al. 2005). As a result, an acute ischemic infarct model was created by disabling active contraction in the AA region of the heart. The intracellular calcium concentration in the infarcted tissue was set to zero ($Ca_0 = 0 \mu\text{mol/l}$) to shut down active contraction. The passive mechanical properties of the cardiac tissue (stress-scaling coefficient C) and the fibre directions were not altered compared to the healthy model. AA ischemic infarct models 2 (II_2) and 3 (II_3) simulate the phase of the infarct healing process in which necrosis (cell death) and degradation of structural proteins result in a decrease in passive mechanical properties of the infarcted myocardium (Holmes et al. 2005). Consequently, the tissue stiffness was set at 50% and 25% of the healthy value by decreasing the stress scaling coefficient C to 0.44 kPa and 0.22 kPa for models 2 and 3, respectively. The AA region was defined as non-contractile ($Ca_0 = 0 \mu\text{mol/l}$), while all other parameters including the wall thickness were identical to the healthy model. Lastly, the AA scarred infarct model (SI) mimics the scar formation in the infarcted region which results in a large increase in tissue stiffness and thinning of the wall (Holmes et al. 2005). The AA scarred infarct was modelled as non-contractile and stiff by increasing the stress scaling coefficient C , 10-fold to 8.8 kPa (Sun et al. 2009). Moreover, the thickness of the AA infarcted wall was reduced from both the endo- and epicardial side corresponding to a total volume of 9.4 ml to simulate wall thinning due to scar formation (Holmes et al 2005). Active contraction of the infarcted tissue was shut down ($Ca_0 = 0 \mu\text{mol/l}$) while all other parameters were not different from the healthy heart model (Dang et al. 2004, 2005; Guccione et al. 2001).

[figure 1]

The hydrogel inclusions were described as a structure of four alternating thin layers into the wall of the AA infarct (Figure 2). This biomaterial configuration was chosen to approximate the multi-layered distribution of the injected biomaterial observed in previous experimental studies (Dobner et al. 2009; Ifkovits et al. 2010). The total volume of the incorporated hydrogel was set at 9.4 ml. This was the same in all models and was added to the volume of the AA infarcted region leading to wall thickening in the infarct models with hydrogel inclusion. Thickness of the AA infarcted wall was increased from both the endo- and epicardial side. The hydrogel volume of 9.4 ml on a total heart wall volume of 141.2 ml in the three ischemic models and 131.8 ml in the scarred model indicated a hydrogel content of 6.7% and 7.1%, respectively.

Mechanical properties of the hydrogel were defined as isotropic. Isotropic material properties were modelled by choosing the same value, 18.5, for the strain and shear coefficients b_{ff} , b_{cc} and b_{fc} , in the strain energy function. The stiffness of the hydrogel was based on a previous study in which a non-degradable biomaterial, polyethylene glycol (PEG) was injected in a rat infarct model (Dobner et al. 2009). Mechanical testing of this gel indicated that the stiffness of the gel was 50% of the stiffness of healthy myocardium (unpublished results). So, the stress scaling coefficient C for healthy myocardium; $C=0.88$ kPa, was reduced with 50% for the hydrogel; $C=0.44$ kPa. Lastly, the hydrogel was modelled as non-contractile ($Ca_0 = 0 \mu\text{mol/l}$). To investigate the effect of a particular AA infarct with or without hydrogel inclusions on the cardiac function, simulations were run for every model, and global cardiac hemodynamics and regional mechanics were investigated.

[figure 2]

2.3 Cardiac hemodynamics

Cardiac hemodynamics were analyzed by computing the pressure-volume relationships of the left ventricle (LV) for the systolic and diastolic phase of the cardiac cycle. The diastolic compliance or passive filling of the LV is represented by the end-diastolic pressure volume relation (EDPVR), while the systolic elastance or contractility of the LV is defined by the end-systolic pressure volume relation (ESPVR). Systolic contractility or elastance (E_{max}) is one of the cardiac functional parameters and is obtained by determining the slope of the ESPVR curve. The dead space volume (V_0) is the volume inside the ventricle which is not able to be ejected and is defined by the volume intercept of the ESPVR curve. The other cardiac functional parameters, stroke volume and ejection fraction were calculated from the pressure – volume (PV) relations by the following equations:

$$SV = V_{ED} - V_{ES} \quad (3)$$

$$EF = \frac{SV}{V_{ED}} \quad (4)$$

in which SV is the stroke volume (ml), V_{ED} is the end-diastolic volume (ml) determined at the end-diastolic pressure of 1.33 kPa (10 mmHg), V_{ES} is the end-systolic volume (ml) assessed at the end-systolic pressure of 13.3 kPa (100 mmHg), and EF is the ejection fraction (-) of the left ventricle.

2.4 Myocardial mechanics

Myofibre stresses in reference to the local muscle fibre orientation were calculated in the left ventricle for the healthy control and the infarct models. Stress values were obtained at the Gaussian points of each element and the average value per element was weighted by the element volume. Myofibre stresses were computed and averaged at end-diastole ($P=10$ mmHg = 1.33 kPa) and end-systole ($P=100$ mmHg = 13.33 kPa). To study the effect of hydrogel injection on extreme stress and strain values in the (infarcted) AA region of the left ventricle, maximum end-diastolic and end-systolic myofibre strains and stresses were calculated for the different models.

3. Results

3.1 Cardiac hemodynamics; Pressure Volume (PV) relationships & cardiac functional parameters

The cardiac hemodynamics of the different heart models were studied by obtaining the end-diastolic and end-systolic PV relationships of each model and calculating the cardiac functional parameters. The PV relationships for the healthy and different infarct models with and without hydrogel layer incorporation in the infarcted wall are shown in figure 3. The

cardiac functional parameters of the healthy and all infarct models were calculated from the PV relationships and are shown in table 1.

[figure 3]

[table 1]

In comparison to the healthy case, a decrease in contractility (E_{max}) of 32%, 37% and 40% is seen in models II_1 , II_2 and II_3 , respectively. A reduction of 20% in contractility is shown in the SI model, relative to the healthy reference. An increase in V_0 of 19%, 19%, 21% and 12% is observed in the II_1 , II_2 , II_3 and SI models, respectively, when compared to the healthy model. The decrease in stroke volume (SV) is similar as seen for the contractility in models II_1 , II_2 , II_3 and SI; 52%, 50%, 48% and 59%, respectively. The ejection fraction (EF) is reduced by 52% in models II_1 , II_2 and II_3 , and by 53% in the SI model compared to the healthy model.

Improvement of cardiac contractility of 14%, 21% 25% and 8% in the II_1G , II_2G , II_3G , and SIG models, respectively, is shown after incorporation of hydrogel in the AA infarcted wall. A decrease of V_0 of 6.5%, 6.0% and 7.4% is seen in the II_1G , II_2G and II_3G models, respectively after hydrogel inclusion in the myocardial wall. In the SIG model, a small increase in V_0 of 1.2% is even observed. Stroke volume values are recovered by 2.0%, 1.3% and 14%, respectively, in the II_1G , II_2G and SIG models. However, no improvement of the stroke volume but a decrease of 1.1% is found in the II_3G model compared to the II_3 model. The ejection fraction of the left ventricle is raised by 10% in II_1G , 12% in II_2G , 12% in II_3G and 14% in SIG, as a result of the hydrogel layer presence in the heart wall.

3.2 Myocardial mechanics; LV myofibre stresses & maximum infarct myofibre stresses and strains

Left ventricular myofibre stresses were calculated and averaged at the end-diastolic (ED) and end-systolic (ES) phases of the cardiac cycle in the different cardiac models. Results are represented in table 2. A decrease of 16%, 22%, 25% and 3.0% in average ED LV myofibre stresses is observed in models II_1G , II_2G , II_3G and SIG respectively, compared to the models without hydrogel. The same phenomenon is seen in the mean ES LV myofibre stresses; a stress reduction of 21%, 27%, 29 % and 2.1% in the II_1G , II_2G , II_3G and SIG models, respectively. In the ischemic models without hydrogel, average ED LV myofibre stresses are indicated which are equal (II_1) and larger (II_2 and II_3) than in the healthy control model. After hydrogel addition, smaller mean ED LV myofibre stresses are found in the ischemic models compared to the healthy control. The same observation is made for the average ES LV myofibre stresses. In the ischemic models without hydrogel, average ES LV myofibre stresses are larger than in the healthy control model. Additionally, smaller mean ES LV myofibre stresses are found in the ischemic models with hydrogel inclusion compared to the healthy control.

[table 2]

The maximum ED and ES myofibre stresses and strains in the AA region of the heart are represented in figure 4. The positive effect of hydrogel inclusion is clearly observed in all three ischemic models. Maximum ED myofibre stress values are decreased with 27%, 45% and 48% respectively in models II_1G , II_2G and II_3G . Moreover, maximum ES myofibre

stresses are reduced with 43%, 54% and 56% respectively in models II₁G, II₂G and II₃G. The same trend is seen for the maximum myofibre strain values in the infarcted tissue in ED but not in ES. A decrease of 5.6%, 4.8% and 8.3% of the maximum ED myofibre strains is observed while maximum ES myofibre strains are increased with 8.0%, 3.4% and 3.0% in the II₁G, II₂G and II₃G models, respectively. In contrast, maximum stresses and ED strain in the infarct region in the SIG model are found to be higher instead of lower due to hydrogel injection; maximum stresses are grown with 53% and 57% and maximum ED strain with 44% while the maximum ES strain is reduced with 14%.

[figure 4]

4. Discussion

Despite the growing literature of experimental research in which biomaterial injection has been applied to improve cardiac functionality after myocardial infarction (Nelson et al. 2011) only a limited number of numerical studies have been performed (Wall et al. 2006, Wenk et al. 2009). In these studies, the definition and distribution of the simulated hydrogel in the infarcted LV wall was simplified and needed to be improved towards in vivo data. Therefore, the objective of this computational study was to examine the effect of a more realistic biomaterial distribution in the infarcted LV wall, on cardiac function and heart wall mechanics.

A validated canine FE heart model was employed in which an antero-apical (AA) infarct was defined. Four infarct models were created representing different temporal phases in the development of a myocardial infarction from the onset of the infarct towards the formation of scar tissue. Multiple hydrogel layers of which the distribution was based on experimental studies were simulated in the infarcted myocardium of each model. Biomechanical and functional improvement of the infarcted LV was found after hydrogel inclusion in the infarct models representing the early phases of myocardial infarction. Only functional improvement was shown in the scar model due to hydrogel presence.

4.1 Cardiac hemodynamics

The pressure-volume diagrams and the derived cardiac functional parameters indicated enhancement of LV functionality due to hydrogel incorporation in the infarcted myocardium in the three ischemic models and in the scar model.

In general, cardiac function is affected by the mechanical properties of the myocardium. A change in mechanical properties of the infarcted myocardium due to hydrogel injection can lead to an improvement in ventricular performance. The mechanical behaviour of the infarcted tissue has a different influence during both phases of the cardiac cycle. During systole, a compliant infarct region hinders contraction as the tissue is stretched, energy of the healthy non-infarcted myocardium is dissipated and the ventricular pump function is reduced (Bogen et al. 1980; Laird and Vellekoop 1977). In contrast, little negative effects of a stiff infarct on cardiac contraction have been found. During diastole, however, a stiff infarct impairs diastolic filling by enlarging the overall ventricular stiffness (Smith et al. 1974). These mechanisms also apply when mechanical properties of the myocardium are changed by injection of biomaterials into the myocardium.

The pressure-volume diagram is commonly used to assess cardiac (LV) functionality. Myocardial infarction affects both the systolic and diastolic functions of the ventricle which

are visualized in the diagram. An increase in stiffness of the LV due to scarring of the myocardium following an infarct, leads to an increase in the slope of the EDPVR requiring increased pressure to enlarge and fill the less-compliant ventricle. In addition, a decrease in LV stiffness leads to a decline in the EDPVR-slope. In the II₂ and II₃ models, a reduced stiffness was defined in the infarcted region and, therefore, the slopes of the EDPVR curves were smaller than that of the healthy control. In model II₁, the same diastolic behaviour as in the healthy control model was obtained since the passive properties of both models were identical. After addition of the hydrogel layers in these models, the stiffness of the infarcted region was increased and the slopes of the EDPVR curves were augmented. An inverse effect should have been seen in the SIG model, an increase in compliance of the myocardium due to addition of a less stiff biomaterial. However, this effect was very small probably due to the relatively small volume of hydrogel included in the LV wall.

The effect of regional infarction on the systolic ventricular function, indicated by the ESPVR curves is less straightforward. The slope of the ESPVR curve representing contractility (E_{max}), not only reflect the contractile state of the non-infarcted muscle, it is also a measure of the net elastance of both infarcted and normal myocardium (Kass et al. 1990). In all infarcted models, active contraction was disabled in the AA region of the heart and, therefore, contractility (E_{max}) of the LV was smaller than in the healthy model. In the II₁, II₂ and II₃ models, the stiffness of the infarcted tissue was equal, 50% and 25%, respectively, of the stiffness of the infarct region in the healthy model. Therefore, ventricular contractility was highest in model II₁ and lowest in II₃. After incorporation of the biomaterial layers, the wall thickness, mechanical properties and, consequently, contractility of the myocardium were increased. The relative increase in contractility was largest for model II₃G and smallest for II₁G. For all three ischemic models the contractility after hydrogel layer inclusion in the myocardial wall seemed to be similar despite the different mechanical properties of the infarct region. This could suggest that independent of the time point of injection but before scar formation, hydrogel layer inclusion would lead to the same improved LV contractility. However, the formation of a layered hydrogel distribution in the infarcted LV wall was only reported to occur in vivo after immediate biomaterial injection following myocardial infarction (Dobner et al 2009; Ifkovits et al. 2010). Consequently, more research is required to investigate if multi-layered gel formation would also result from biomaterial injection in the infarcted cardiac tissue at different time points after the onset of infarction.

In the scar model, the contractility of the ventricular myocardium was in between the contractility values found in the healthy and ischemic models. Of all models, stiffness of the infarct region was highest in the scar model and this resulted in the smallest reduction in contractility compared to the healthy model. In the scar model, the effect of hydrogel layer inclusion in the LV wall was smaller than in the ischemic models, but it still led to an increase in contractility. The substitution of a part of the scarred infarct region by a less stiff material would have lowered the overall stiffness and contractility of the ventricular wall. However, the hydrogel inclusion was responsible for an increase in wall thickness resulting in a rise in overall stiffness and, consequently, a larger contractility in the scarred infarct model.

In the ischemic models, the positive effect of hydrogel layer incorporation in the LV wall on dead space volume (V_0) was clearly visible, while in the SIG model a slightly adverse effect was observed. From literature it is known that the effect of regional infarction on the PV diagram results in a rightward shift of the ESPVR curves due to an increase in V_0 along the volume axis (Kass et al. 1990; Sunagawa et al. 1983). This shift is explained by the passive stretching of the infarcted tissue when active contraction is disabled. It leads to an enlarged dead space volume due to regional bulging within the ventricle wall. This volume is displaced inside the ventricle but is not able to be ejected. The magnitude of the rightward shift of the ESPVR curve correlates with the proportion of ventricle that has become

infarcted. Since the size of the infarcted region was identical in the ischemic infarct models (II₁, II₂ and II₃), the difference in the rightward shift of V_0 for these models resulted from the difference in mechanical properties of the infarcted region. When the mechanical properties of the myocardial infarct are lower, stretching of the ventricular wall is larger resulting in a larger rightward shift of V_0 .

The presented leftward shift of the V_0 curves of all infarct models after hydrogel inclusion seemed to be dominated by the geometric change of the LV due to the hydrogel layer incorporation, which led to an increase in LV wall volume and a decrease in LV cavity volume. The effect of the change in mechanical properties due to the hydrogel, appeared to be less since the dead space volumes were similar in the three ischemic models with hydrogel addition.

4.2 Myocardial mechanics

The mechanical analyses showed that the inclusion of hydrogel layers into the infarcted myocardial wall led to a decline in mean LV myofibre stresses and maximum myofibre stresses in all ischemic cardiac models. This is a positive effect since high stresses in the heart wall can lead to progressive structural and functional changes in the heart muscle predisposing towards the end stage of cardiac failure (Baig et al. 1999). In contrast to the results with regard to ventricular performance, the addition of hydrogel layers in the scar model did not positively affect the cardiac mechanics.

The mean LV myofibre stress level reduction due to hydrogel incorporation was 21 - 29% for ES and 16 - 25% for ED in the ischemic infarct models. This reduction was larger as seen in a previous FE study in which the most optimal pattern of polymer inclusions in the LV wall led to a decrease in mean LV myofibre stress of 5% and 15%, respectively, for ES and ED when compared with the model without inclusions (Wenk et al. 2009). While the dimensions of the LV geometry in both studies were similar (in both cases a dog model was used), the amount and distribution of the hydrogel inclusions were considerably different. In this study, a layered hydrogel configuration with a total volume of 9.4 ml was modelled whereas in the previous FE study, the biomaterial incorporation was simulated by spherical polymers having an overall volume of 5.2 ml (Wenk et al. 2009). It has been shown before that the mean myofibre stress in the LV reduces as the injected biomaterial volume is larger (Wall et al. 2006; Wenk et al. 2009). This may be the reason for the larger stress reduction due to hydrogel addition seen in this study.

The stress results showed that the presence of an AA infarct into the LV wall led to an overall increase in mean LV myofibre stress in all infarct models, i.e. the mean LV myofibre stress in the healthy model was smaller than in the infarct models. This was in correspondence with previous studies (Walker et al. 2005; Dang et al. 2005; Wenk et al. 2011). Moreover, the incorporation of hydrogel layers in the infarcted LV wall resulted in strongly reduced mean LV myofibre stresses in the three ischemic infarct models, while the decrease in stresses was relatively small in the scarred infarct model. Generally, an increase in wall volume is known to reduce mean wall stresses. However, since the amount of hydrogel added to the infarcted LV wall was identical in all infarct models, it does not explain the difference in stress level reduction. This difference was caused by the difference in mechanical properties between the hydrogel and the infarcted regions in the varying models. When the stiffness of the added hydrogel is relatively large compared to the stiffness of the surrounding myocardial tissue, the hydrogel will bear a larger extent of the force exerted to the LV wall resulting in a larger drop of the stress levels in the LV myocardium.

Maximum myofibre stresses and strains in the infarcted region in the ischemic models were generally found to be lowered due to hydrogel incorporation. Both the calculated maximum stresses and strains give an indication of the risk of infarct rupture since this is characterized by thinning and bulging of the ventricular wall (Schuster and Bulkley 1979). It accounts for 10–20% of all in-hospital deaths due to acute myocardial infarction (Becker et al. 1996; Lopez-Sendon et al. 1992). Within the first week after the onset of infarction, the risk of heart wall rupture is highest (Birnbaum et al. 2003; Wehrens and Doevendans 2004). Since the ischemic models represented this time period, the results suggested that hydrogel layer incorporation in the cardiac wall reduced the risk of rupture of the infarcted myocardium.

4.3 Cardiac and myocardial modelling

In the ischemic models II_1 , II_2 and II_3 , the wall thickness of the infarcted zone was set equal to the myocardial wall thickness in the healthy model. In literature, wall thinning of the infarcted region was observed after myocardial infarction (Holmes et al. 2005). However, the ischemic models represented the relatively short time period of one week after the onset of infarction in which reduction in infarcted wall thickness was limited [unpublished results]. In contrast, a myocardial infarction of at least three weeks old was simulated in the SI model. The presence of a thinner infarct wall in this scar model was according to literature (Fujimoto et al. 2009; Jiang et al. 2009; Yoon et al. 2009).

In the infarct models, the direction and magnitude of the fibre angles in the healthy tissue were unaltered in the ischemic or scar tissue. This was based on previous computational studies in which the fibre direction and the magnitude of the fibre strain, cross-fibre strain and shear coefficients were kept constant for healthy, border zone and aneurysmal tissue in the myocardial infarct models (Dang et al. 2004; Guccione et al. 2001, 2005; Wenk et al. 2010). In other FE studies, the material coefficients representing the magnitude of the fibre angle were determined with an iterative process from experimental data (tagged MRI measurements). At the aneurysm region, fibre angles were set to zero degrees in order to use experimentally determined infarct material parameters with respect to this direction. Results showed different values of the material parameters indicating anisotropy in the infarcted myocardium dissimilar to the healthy tissue (Walker et al. 2005, 2008). In experimental studies, consistency has not been found about the structure and mechanics of a myocardial infarction and, thus, about the direction and magnitude of fibre angles in infarcted tissue. In a rat model, healing infarcts appeared to be structurally and mechanically isotropic at 1, 2, 3 and 6 weeks after coronary ligation (Fomovsky and Holmes 2010). On the contrary, quantitative structural analysis of healing pig (Holmes and Covell 1996) and dog (Whittaker et al. 1989) scars showed a high degree of collagen fibre alignment, with mean orientation in the circumferential direction. In addition, sheep scars were found to be mechanically anisotropic, with a degree and direction of anisotropy that changed over time (Gupta et al. 1994). Overall, it seems that more research is needed into the structure and mechanics of a myocardial infarction developing in time. With this information it would be possible to get a better insight in the effect of infarct properties on ventricular performance.

The dispersion of the hydrogel in the infarcted heart wall was modelled as multiple thin layers. This distribution was based on experimental work in which the injection of a non-degradable gel resulted in a layered hydrogel structure in the infarcted cardiac region after 4 and 13 weeks in rats (Dobner et al. 2009), and after 8 weeks in sheep (Ifkovits et al. 2010) In previous FE studies, the hydrogel injection in the infarcted LV was modelled as somewhat unrealistic spherical inclusions (Wenk et al. 2009) or without any specific geometry or

distribution (Wall et al. 2006). The current FE study is the first one, to our knowledge, in which the hydrogel configuration in the LV infarcted wall was directly based on experimental work. However, the representation of the experimentally observed layered hydrogel distribution was simplified in the model, and further improvement would still be possible and desired to optimize the coupling between experimental and numerical work.

5. Acknowledgements

Jeroen Kortsmits acknowledges the Claude Leon Foundation for financial support in form of a post-doctoral fellowship. Renee Miller received a Whitaker fellowship. The internship of Jesse R. Macadangdang was supported from the National Science Foundation, USA.

6. References

Baig MK, Mahon N, McKenna WJ, Caforio ALP, Bonow RO, Francis GS. 1999. The pathophysiology of advanced heart failure. *Heart and Lung*. 28(2):87-101.

Becker R, Gore J, Lambrew C, Weaver W, Rubison R, French W, Tiefenbrunn A, Bowlby L, Rogers W. 1996. A composite view of cardiac rupture in the United States National Registry of Myocardial Infarction. *J Am Coll Cardiol*. 27(6):1321-1326.

Birnbaum Y, Chamoun AJ, Anzuini A, Lick SD, Ahmad M, Uretsky BF. 2003. Ventricular free wall rupture following acute myocardial infarction. *Coronary Artery Disease*. 14(6):463-470.

Bogen DK, Rabinowitz SA, Needleman A, McMahan TA, Abelmann WH. 1980. An analysis of the mechanical disadvantage of myocardial infarction in the canine left ventricle. *Circ Res*. 47(5):728-741.

Bovendeerd PH, Arts T, Delhaas T, Huyghe JM, van Campen DH, Reneman RS. 1996. Regional wall mechanics in the ischemic left ventricle: numerical modeling and dog experiments. *American Journal of Physiology - Heart and Circulatory Physiology*. 270(1):H398-H410.

Cardiovascular diseases (CVDs) - Key Facts. 2011. WHO. Fact sheet 317. Available from <http://www.who.int>.

Dang ABC, Guccione JM, Mishell JM, Zhang P, Wallace AW, Gorman RC, Gorman JH, Ratcliffe MB. 2004. Akinetic segments of myocardial infarction contain contracting myocytes: A finite element model study. *Journal of the American College of Cardiology*. 43(5):177a-177a.

Dang ABC, Guccione JM, Mishell JM, Zhang P, Wallace AW, Gorman RC, Gorman JH, Ratcliffe MB. 2005. Akinetic myocardial infarcts must contain contracting myocytes: finite-element model study. *American Journal of Physiology-Heart and Circulatory Physiology*. 288(4):H1844-H1850.

Dang ABC, Guccione JM, Zhang P, Wallace AW, Gorman RC, Gorman JH, Ratcliffe MB. 2005. Effect of ventricular size and patch stiffness in surgical anterior ventricular restoration: A finite element model study. *Annals of Thoracic Surgery*. 79(1):185-193.

Dobner S, Bezuidenhout D, Govender P, Zilla P, Davies N. 2009. A Synthetic Non-degradable Polyethylene Glycol Hydrogel Retards Adverse Post-infarct Left Ventricular Remodeling. *Journal of Cardiac Failure*. 15(7):629-636.

Fomovsky GM, Holmes JW. 2010. Evolution of scar structure, mechanics, and ventricular function after myocardial infarction in the rat. *American Journal of Physiology-Heart and Circulatory Physiology*. 298(1):H221-H228.

Fujimoto KL, Ma Z, Nelson DM, Hashizume R, Guan J, Tobita K, Wagner WR. 2009. Synthesis, characterization and therapeutic efficacy of a biodegradable, thermoresponsive hydrogel designed for application in chronic infarcted myocardium. *Biomaterials*. 30(26):4357-4368.

Guccione JM, McCulloch AD, Waldman LK. 1991. Passive Material Properties of Intact Ventricular Myocardium Determined From a Cylindrical Model. *Journal of Biomechanical Engineering*. 113(1):42-55.

Guccione JM, McCulloch AD. 1993. Mechanics of Active Contraction in Cardiac-Muscle .1. Constitutive Relations for Fiber Stress That Describe Deactivation. *Journal of Biomechanical Engineering-Transactions of the Asme*. 115(1):72-81.

Guccione JM, Costa KD, McCulloch AD. 1995. Finite element stress analysis of left ventricular mechanics in the beating dog heart. *J Biomech*. 28(10):1167-1177.

Guccione JM, Moonly SM, Moustakidis P, Costa KD, Moulton MJ, Ratcliffe MB, Pasque MK. 2001. Mechanism underlying mechanical dysfunction in the border zone of left ventricular aneurysm: A finite element model study. *Annals of Thoracic Surgery*. 71(2):654-662.

Guccione JM, Salahieh A, Moonly SM, Kortsmitt J, Wallace AW, Ratcliffe MB. 2003. Myosplint decreases wall stress without depressing function in the failing heart: a finite element model study. *Ann Thorac Surg*. 76(4):1171-1180.

Gupta K, Ratcliffe M, Fallert M, Edmunds L, Jr, Bogen D. 1994. Changes in passive mechanical stiffness of myocardial tissue with aneurysm formation. *Circulation*. 89(5):2315-2326.

Heart Disease and Stroke statistics. 2008. American Heart Association. Dallas.

Holmes JW, Covell JW. 1996. Collagen fiber orientation in myocardial scar tissue. *Cardiovascular Pathobiology*. 1:15-22.

Holmes JW, Borg TK, Covell JW. 2005. Structure and mechanics of healing myocardial infarcts. *Annual Review of Biomedical Engineering*. 7:223-253.

Ifkovits JL, Tous E, Minakawa M, Morita M, Robb JD, Koomalsingh KJ, Gorman JH, Gorman RC, Burdick JA. 2010. Injectable hydrogel properties influence infarct expansion

and extent of postinfarction left ventricular remodeling in an ovine model. *Proceedings of the National Academy of Sciences of the United States of America*. 107(25):11507-11512.

Jiang XJ, Wang T, Li XY, Wu DQ, Zheng ZB, Zhang JF, Chen JL, Peng B, Jiang H, Huang C, et al. 2009. Injection of a novel synthetic hydrogel preserves left ventricle function after myocardial infarction. *J Biomed Mater Res A*. 90(2):472-477.

Kass D, Midei M, Brinker J, Maughan W. 1990. Influence of coronary occlusion during PTCA on end-systolic and end-diastolic pressure-volume relations in humans. *Circulation*. 81(2):447-460.

Kawamoto A, Tkebuchava T, Yamaguchi J, Nishimura H, Yoon YS, Milliken C, Uchida S, Masuo O, Iwaguro H, Ma H, et al. 2003. Intramyocardial transplantation of autologous endothelial progenitor cells for therapeutic neovascularization of myocardial ischemia. *Circulation*. 107(3):461-468.

Kerckhoffs RC, Neal ML, Gu Q, Bassingthwaite JB, Omens JH, McCulloch AD. 2007. Coupling of a 3D finite element model of cardiac ventricular mechanics to lumped systems models of the systemic and pulmonary circulation. *Ann Biomed Eng*. 35(1):1-18.

Klodell Jr CT, Aranda Jr JM, McGiffin DC, Rayburn BK, Sun B, Abraham WT, Pae Jr WE, Boehmer JP, Klein H, Huth C. 2008. Worldwide surgical experience with the Paracor HeartNet cardiac restraint device. *The Journal of Thoracic and Cardiovascular Surgery*. 135(1):188-195.

Laird JD, Vellekoop HP. 1977. The course of passive elasticity of myocardial tissue following experimental infarction in rabbits and its relation to mechanical dysfunction. *Circ Res*. 41(5):715-721.

Lopez-Sendon J, Gonzalez A, Lopez de Sa E, Coma-Canella I, Roldan I, Dominguez F, Maqueda I, Martin Jadraque L. 1992. Diagnosis of subacute ventricular wall rupture after acute myocardial infarction: sensitivity and specificity of clinical, hemodynamic and echocardiographic criteria. *J Am Coll Cardiol*. 19(6):1145-1153.

Nelson DM, Ma Z, Fujimoto KL, Hashizume R, Wagner WR. 2011. Intra-myocardial biomaterial injection therapy in the treatment of heart failure: Materials, outcomes and challenges. *Acta Biomaterialia*. 7(1):1-15.

Nielsen PM, Le Grice IJ, Smaill BH, Hunter PJ. 1991. Mathematical model of geometry and fibrous structure of the heart. *American Journal of Physiology - Heart and Circulatory Physiology*. 260(4):H1365-H1378.

Omens JH, MacKenna DA, McCulloch AD. 1993. Measurement of strain and analysis of stress in resting rat left ventricular myocardium. *Journal of Biomechanics*. 26(6):665-676.

Pfeffer M, Pfeffer J. 1987. Ventricular enlargement and reduced survival after myocardial infarction. *Circulation*. 75(5 Pt 2):IV93-97.

Pfeffer M, Braunwald E. 1990. Ventricular remodeling after myocardial infarction. Experimental observations and clinical implications. *Circulation*. 81(4):1161-1172.

- Schuster E, Bulkley B. 1979. Expansion of transmural myocardial infarction: a pathophysiologic factor in cardiac rupture. *Circulation*. 60(7):1532-1538.
- Smith M, Russell RO, Jr., Feild BJ, Rackley CE. 1974. Left ventricular compliance and abnormally contracting segments in postmyocardial infarction patients. *Chest*. 65(4):368-378.
- Steyn K, Sliwa K, Hawken S, Commerford P, Onen C, Damasceno A, Ounpuu S, Yusuf S. 2005. Risk Factors Associated With Myocardial Infarction in Africa: The INTERHEART Africa Study. *Circulation*. 112(23):3554-3561.
- Sun K, Stander N, Jhun CS, Zhang ZH, Suzuki T, Wang GY, Saeed M, Wallace AW, Tseng EE, Baker AJ, et al. 2009. A Computationally Efficient Formal Optimization of Regional Myocardial Contractility in a Sheep With Left Ventricular Aneurysm. *Journal of Biomechanical Engineering-Transactions of the Asme*. 131(11):111001-1-10.
- Sunagawa K, Maughan W, Sagawa K. 1983. Effect of regional ischemia on the left ventricular end-systolic pressure-volume relationship of isolated canine hearts. *Circ Res*. 52(2):170-178.
- Sutton MG, Sharpe N. 2000. Left ventricular remodeling after myocardial infarction: pathophysiology and therapy. *Circulation*. 101(25):2981-2988.
- Tischler MD, Niggel J, Borowski DT, Lewinter MM. 1993. Relation between left ventricular shape and exercise capacity in patients with left ventricular dysfunction. *Journal of the American College of Cardiology*. 22(3):751-757.
- Usyk TP, Mazhari R, McCulloch AD. 2000. Effect of laminar orthotropic myofiber architecture on regional stress and strain in the canine left ventricle. *Journal of Elasticity*. 61(1-3):143-164.
- Walker JC, Ratcliffe MB, Zhang P, Wallace AW, Fata B, Hsu EW, Saloner D, Guccione JM. 2005. MRI-based finite-element analysis of left ventricular aneurysm. *Am J Physiol Heart Circ Physiol*. 289(2):H692-700.
- Walker JC, Ratcliffe MB, Zhang P, Wallace AW, Hsu EW, Saloner DA, Guccione JM. 2008. Magnetic resonance imaging-based finite element stress analysis after linear repair of left ventricular aneurysm. *Journal of Thoracic and Cardiovascular Surgery*. 135(5):1094-U1057.
- Wall ST, Walker JC, Healy KE, Ratcliffe MB, Guccione JM. 2006. Theoretical impact of the injection of material into the myocardium: a finite element model simulation. *Circulation*. 114(24):2627-2635.
- Wehrens XHT, Doevendans PA. 2004. Cardiac rupture complicating myocardial infarction. *International journal of cardiology*. 95(2):285-292.
- Wenk JF, Wall ST, Peterson RC, Helgerson SL, Sabbah HN, Burger M, Stander N, Ratcliffe MB, Guccione JM. 2009. A Method for Automatically Optimizing Medical Devices for Treating Heart Failure: Designing Polymeric Injection Patterns. *Journal of Biomechanical Engineering-Transactions of the Asme*. 131(12):121011-1-7.
- Wenk JF, Zhang ZH, Cheng GM, Malhotra D, Acevedo-Bolton G, Burger M, Suzuki T, Saloner DA, Wallace AW, Guccione JM, et al. 2010. First Finite Element Model of the Left

Ventricle With Mitral Valve: Insights Into Ischemic Mitral Regurgitation. *Annals of Thoracic Surgery*. 89(5):1546-1554.

Wenk JF, Sun K, Zhang Z, Soleimani M, Ge L, Saloner D, Wallace AW, Ratcliffe MB, Guccione JM. 2011. Regional left ventricular myocardial contractility and stress in a finite element model of posterobasal myocardial infarction. *J Biomech Eng*. 133(4):044501-6.

White H, Norris R, Brown M, Brandt P, Whitlock R, Wild C. 1987. Left ventricular end-systolic volume as the major determinant of survival after recovery from myocardial infarction. *Circulation*. 76(1):44-51.

Whittaker P, Boughner DR, Kloner RA. 1989. Analysis of healing after myocardial infarction using polarized light microscopy. *American Journal of Pathology*. 134(4):879-893.

Yoon SJ, Fang YH, Lim CH, Kim BS, Son HS, Park Y, Sun K. 2009. Regeneration of ischemic heart using hyaluronic acid-based injectable hydrogel. *Journal of Biomedical Materials Research Part B: Applied Biomaterials*. 91B(1):163-171.

Table 1: Cardiac functional parameters contractility (E_{\max}), dead space volume (V_0), stroke volume (SV) and ejection fraction (EF) for the different models.

Model		Cardiac functional parameters			
		E_{\max} (kPa/ml)	V_0 (ml)	SV (ml)	EF (-)
Healthy Control	H	1.158	15.5	15.7	0.368
Ischemic Infarct 1	II ₁	0.787	18.4	7.48	0.175
Ischemic Infarct 1 + Hydrogel	II ₁ G	0.898	17.2	7.63	0.192
Ischemic Infarct 2	II ₂	0.724	18.4	7.82	0.175
Ischemic Infarct 2 + Hydrogel	II ₂ G	0.874	17.3	7.92	0.196
Ischemic Infarct 3	II ₃	0.693	18.8	8.19	0.177
Ischemic Infarct 3 + Hydrogel	II ₃ G	0.863	17.4	8.10	0.198
Scarred Infarct	SI	0.930	17.3	6.50	0.171
Scarred Infarct + Hydrogel	SIG	1.011	17.5	7.41	0.195

Table 2: Mean left ventricle myofibre stresses (kPa) calculated at the end-diastolic (ED) and end-systolic (ES) time points of the cardiac cycle for the different models.

Model		Mean LV myofibre stress (kPa)	
		ED	ES
Healthy Control	H	1.71	16.54
Ischemic Infarct 1	II ₁	1.71	19.45
Ischemic Infarct 1 + Hydrogel	II ₁ G	1.43	15.46
Ischemic Infarct 2	II ₂	1.81	21.20
Ischemic Infarct 2 + Hydrogel	II ₂ G	1.42	15.58
Ischemic Infarct 3	II ₃	1.90	22.19
Ischemic Infarct 3 + Hydrogel	II ₃ G	1.42	15.70
Scarred Infarct	SI	1.67	18.76
Scarred Infarct + Hydrogel	SIG	1.62	18.36

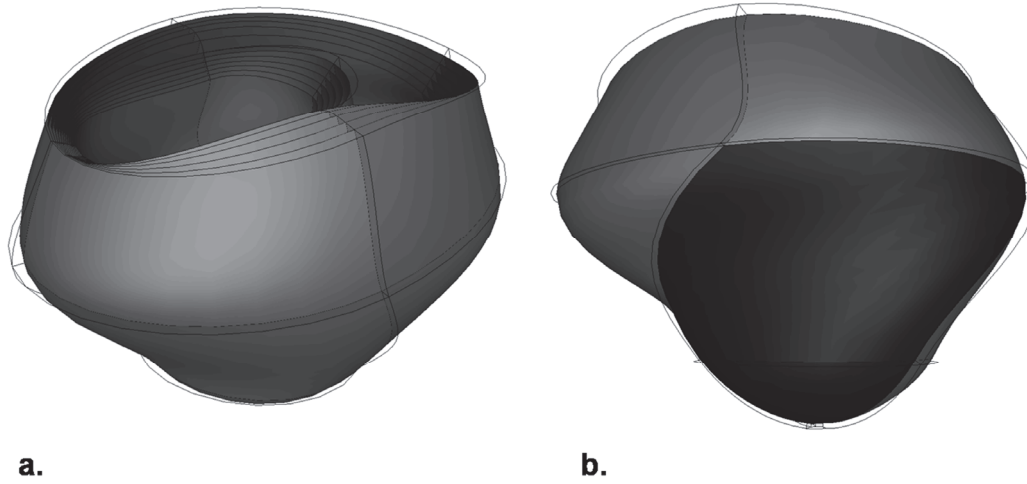


Figure 1: 3D mesh of the canine heart model, a) healthy heart, b) heart with antero-apical (AA) infarct showing the infarct region in black (from a different viewpoint).

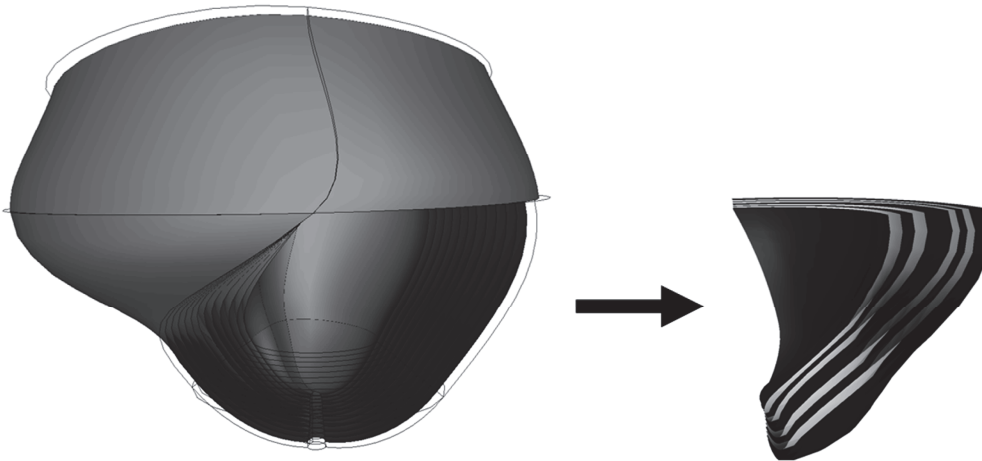


Figure 2: 3D mesh of the canine heart model showing the four alternating thin hydrogel layers (in white) incorporated in the AA infarct wall (in black) in the scarred infarct model (SIG).

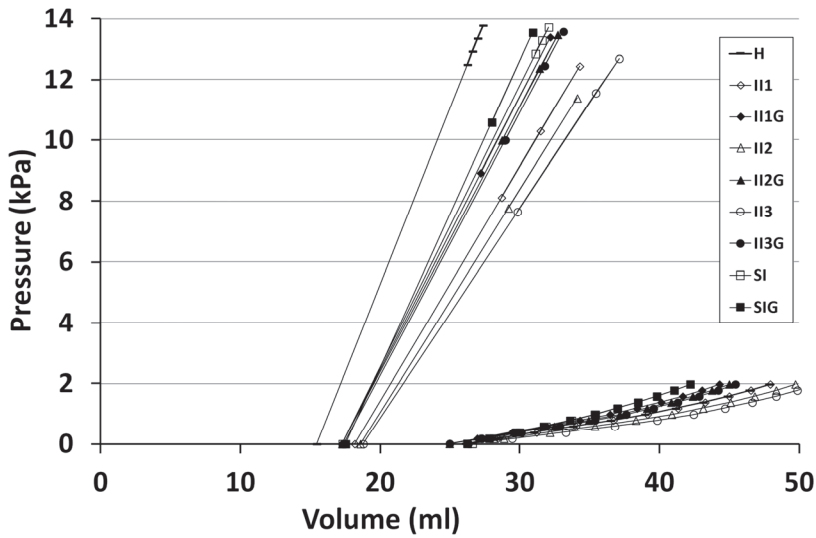


Figure 3: Pressure (kPa) – volume (ml) relationship for the healthy and different infarct models with and without hydrogel layer inclusion. The curves on the left represent the systolic elastance or contractility and the curves on the right, the diastolic compliance of the left ventricle.

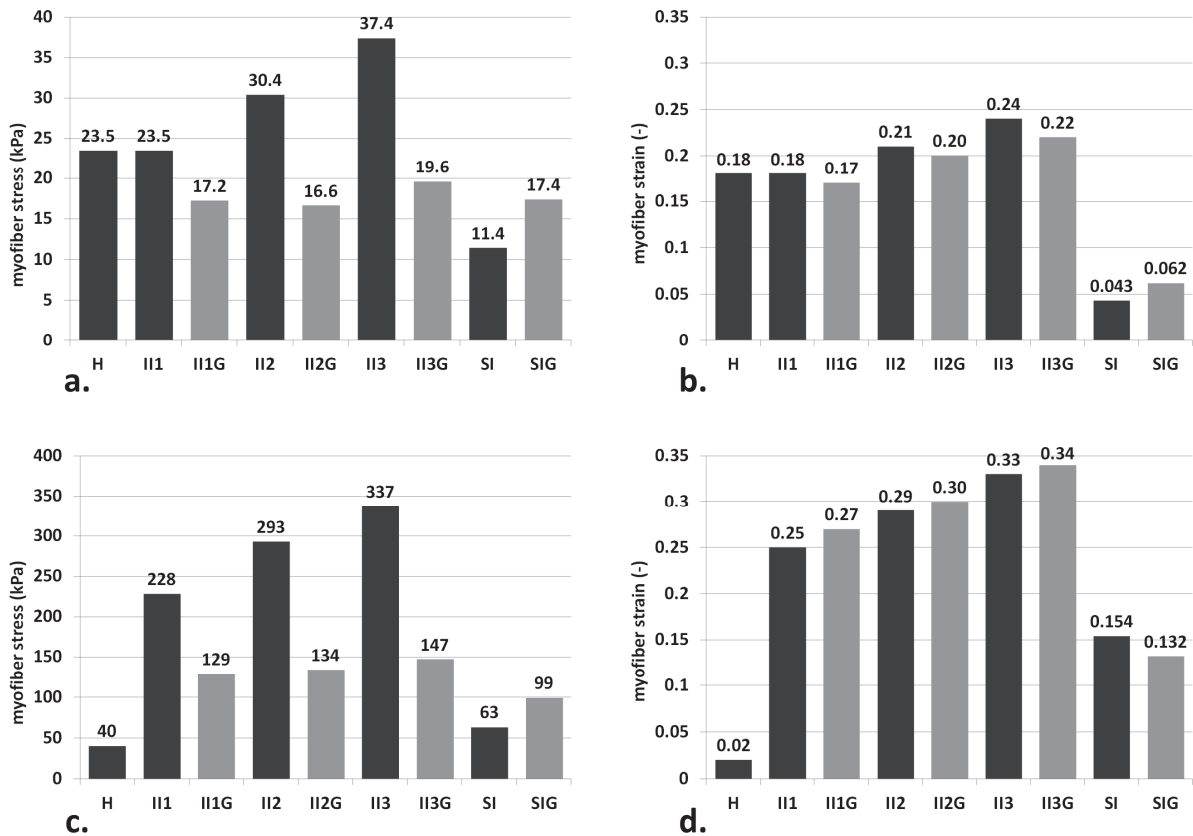


Figure 4: Maximum ED and ES myofibre stresses and strains in the AA region of the heart for the healthy and different infarct models with and without hydrogel layer inclusion, a) maximum ED myofibre stresses, b) maximum ED myofibre strains, c) maximum ES myofibre stresses, d) maximum ES myofibre strains.